ACS APPLIED MATERIALS & INTERFACES

RESEARCH ARTICLE

www.acsami.org

Preparation and Properties of Biodegradable Poly(L-lactide)/ Octamethyl-Polyhedral Oligomeric Silsesquioxanes Nanocomposites with Enhanced Crystallization Rate via Simple Melt Compounding

Jing Yu and Zhaobin Qiu*

State Key laboratory of Chemical Resource Engineering, Key Laboratory of Carbon Fiber and Functional Polymers, Ministry of Education, Beijing University of Chemical Technology, Beijing 100029, China

ABSTRACT: Biodegradable poly(L-lactide) (PLLA)/octamethyl-polyhedral oligomeric silsesquioxanes (ome-POSS) nanocomposites were prepared via simple melt compounding at various ome-POSS loadings in this work. Scanning and transmission electron microscopy observations indicate that ome-POSS were homogeneously dispersed in the PLLA matrix. Effect of ome-POSS on the nonisothermal crystallization behavior, isothermal melt crystallization kinetics, spherulitic morphology, crystal structure, dynamic mechanical properties, and thermal stability of PLLA in the nanocomposites was investigated in detail. It is found that the presence of ome-POSS enhances both nonisothermal cold and melt crystallization of PLLA in the nanocomposites relative to neat PLLA. The overall isothermal melt crystallization rates are faster in the PLLA/ome-POSS nanocomposites than in neat PLLA and increase with increasing the ome-POSS loading; however, the crystallization mechanism of PLLA remains unchanged. The nucleation density of PLLA spherulites is enhanced, while the crystal structure of PLLA is not modified in the PLLA/ome-POSS nanocomposites. The storage modulus has been apparently improved in the PLLA/ome-POSS nanocomposites with respect to neat PLLA, whereas the glass-transition temperatures vary slightly between neat PLLA and the PLLA/ome-POSS nanocomposites. The thermal stability of PLLA matrix is reduced slightly in the PLLA/ome-POSS nanocomposites.

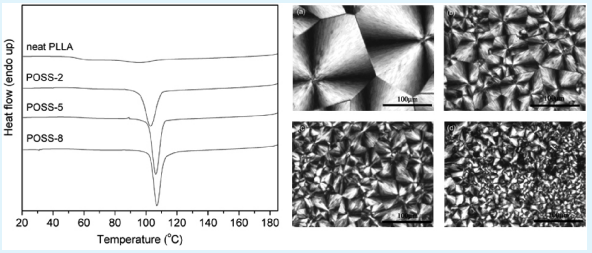

KEYWORDS: poly(L-lactic acid), octamethyl-polyhedral oligomeric silsesquioxanes, morphology, crystalliztion behavior, polymer nanocomposites

INTRODUCTION

Poly(L-lactic acid) (PLLA) is a biodegradable and biocompatible thermoplastic polymer with high strength and high modulus, which has been widely used in the biomedical, agricultural, and general-purpose plastics fields.[1−4] PLLA is also a typical semicrystalline polymer. Three crystal modifications, including α, β, and γ forms, have been reported for PLLA depending on different crystallization conditions.[5,6] Crystallization from the melt usually leads to α form, which is the most common polymorph. Recently, a new crystal modification α′, defined as a disordered modification of the α form, has been discovered and has drawn so much attention.[7−14] The formation of the metastable α′-form crystals of PLLA is kinetically preferential, while that of the thermally stable α-form crystals is thermodynamically favored.[10] It has been found that the disordered α′ and ordered α phases are formed at low (T_c < 100 °C) and high (T_c > 120 °C) crystallization temperatures, respectively.[7−13] However, PLLA has some disadvantages that restrict its practical applications such as poor mechanical properties, slow crystallization rate, and slow degradation rate.[14,15] Therefore, several methods have been developed to overcome the disadvantages, including copolymer synthesis, polymer blending, and chemical grafting methods.[16−21] Recently, the incorporation of nanoparticles such as clay and carbon nanotubes (CNT) into PLLA matrix has been developed as one of the most effective ways to improve the properties of PLLA since nanoparticles can significantly enhance the properties of PLLA even at a very low content. Studies on the PLLA/CNT nanocomposites show that the crystallization of PLLA is accelerated, the hydrolytic degradation of PLLA is enhanced, and the mechanical and thermal properties are improved after nanocomposites preparation.[22−25] The PLLA/clay nanocomposites represent an interesting class of materials due to the variety of structural forms (intercalated, exfoliated, and mixed), leading to significant improvement of the physical properties.[26−29]

The new three-dimensional nanofiller polyhedral oligomeric silsesquioxanes (POSS) contain a cube-like core (Si_8O_{12}) and eight organic groups[30] and may be used for the preparation of higher performance nanostructured organic−inorganic composites in comparison with other inorganic nanofillers.[31,32] POSS molecules can be introduced into polymer matrix via copolymerization and physical blending. Copolymerization is an efficient approach for the preparation of polymer/POSS nanocomposites, through which POSS with reactive functional groups may form chemical bonds or chemical link with the monomer, and thus can raise glass transition temperature, enhance mechanical performance

Received: December 19, 2010
Accepted: February 14, 2011
Published: March 01, 2011

dx.doi.org/10.1021/am1012485 | ACS Appl. Mater. Interfaces 2011, 3, 890–897

and improve thermal stability of polymer.[33−40] However, because of the advantages of low cost and easy industrial implementation, polymer blending and nanocomposites preparation also draw much attention. A majority of polymers blended with POSS have been reported such as polyethylene (PE), polypropylene (PP), poly(methyl methacrylate) (PMMA), poly(methylvinylsiloxane) (PMVS) elastomers, and polyimide (PI).[41−46]

In our previous works,[47,48] biodegradable PLLA/octaisobutyl-polyhedral oligomeric silsesquioxanes (oib-POSS) nanocomposites were prepared by both solution casting method and solution and coagulation method. It is found that PLLA/oib-POSS nanocomposites prepared via solution and coagulation method could get a better dispersion of POSS than those prepared by solution casting. However, despite the different preparation methods, the incorporation of oib-POSS has significantly enhanced the crystallization rate, improved mechanical properties, and accelerated the hydrolytic degradation of PLLA in the nanocomposites with respect to neat PLLA.[47,48]

In this work, biodegradable PLLA/octamethyl-polyhedral oligomeric silsesquioxanes (ome-POSS) nanocomposites were prepared at various ome-POSS loadings ranging from 2 to 8 wt % via simple melt compounding method; moreover, the influence of ome-POSS on the morphology, crystallization, mechanical properties, and thermal degradation of PLLA was investigated in detail with various techniques. It is expected that the research reported herein will be of interest for a better understanding of the structure and properties relationship of biodegradable polymer nanocomposites and may be of help for extending their practical application.

EXPERIMENTAL SECTION

Materials. PLLA (M_w = 1.53 × 10^5 g/mol) was kindly provided by Biomer Company, Germany. Ome-POSS was purchased from Sigma-Aldrich (Shanghai) Trading Co., Ltd.

Preparation of PLLA/ome-POSS Nanocomposites. The PLLA/ome-POSS nanocomposites were prepared via a simple melt compounding method using a melting mixer (MS-II) (Beihang University) at 180 °C for 15 min with a screw speed of 210 rpm. For the fabrication of PLLA/ome-POSS nanocomposites, PLLA was mixed with the addition of various ome-POSS contents, specified as 2, 5, and 8 wt % in the polymer matrix, respectively. For brevity, the nanocomposites containing 2, 5, and 8 wt % ome-POSS are abbreviated as POSS-2, POSS-5, and POSS-8 from now on.

Scanning Electron Microscopy (SEM). A Hitachi S-4700 SEM was used to observe the morphology of the fracture surfaces of the PLLA/ome-POSS nanocomposites. The samples were molded into film at 190 °C and fractured into liquid nitrogen. All specimens were coated with gold before examination.

Transmission Electron Microscopy (TEM). TEM observation was performed with a Hitachi H-800 TEM instrument under an acceleration voltage of 200 kV. Thin sections (with thickness of about 50−70 nm) for TEM observations were cut from the as-prepared nanocomposites under cryogenic conditions (−80 °C) using a Leica EM FC6 ultramicrotome.

Differential Scanning Calorimetry (DSC). Thermal analysis was carried out using a TA Instruments DSC Q100 with a Universal Analysis 2000. All operations were performed under nitrogen purge, and the weight of the samples varied between 4 and 6 mg. For nonisothemal cold crystallization, the sample was heated to 190 at 20 °C/min, held for 3 min to erase any thermal history, cooled to 20 at 40 °C/min to reach the amorphous state, and then heated to 190 °C again at 20 °C/min. The glass transition temperature, the cold crystallization onset temperature, cold crystallization peak temperature, and melting point temperature of neat PLLA and its nanocomposites were read from the second heating traces. For nonisothermal melt crystallization, the sample was heated to 190 at 20 °C/min, held for 3 min to erase any thermal history, and cooled to 20 °C at 5 or 15 °C/min. The crystallization peak temperature was read from the cooling process. For isothermal melt crystallization, the sample was heated to 190 at 20 °C/min, held for 3 min to erase any thermal history, cooled to the chosen crystallization temperature at 40 °C/min, and held for a period of time until the isothermal crystallization was complete. The crystallization temperatures chosen in this work were from 119 to 127 °C. The evolution of heat flow with crystallization time was recorded during the isothermal crystallization process for the later data analysis.

Polarized Optical Microscopy (POM). An optical microscope (Olympus BX51) equipped with a temperature controller (Linkam THMS 600) was used to investigate the spherulitic morphology of neat PLLA and the PLLA/ome-POSS nanocomposites. The samples were first annealed at 190 °C for 3 min and then cooled at 60 °C/min to 125 °C.

Wide-Angle X-ray Diffraction (WAXD). WAXD experiments were performed on a Rigaku D/Max 2500 VB2t/PC X-ray Diffractometer at room temperature in the range of 5−40° with a scanning rate of 4 °/min. The CuKα radiation (λ = 0.15418 nm) source was operated at 40 kV and 200 mA. The samples were first pressed into films with a thickness of around 0.6 mm on a hot stage at 190 °C and then transferred into a vacuum oven at 128 °C for 3 days.

Dynamic Mechanical Analysis (DMA). DMA experiments were performed on the samples of 42 mm × 6 mm × 0.2 mm in size using a dynamic mechanical analyzer of Netzsh DMA242C under tension film mode in the temperature range of 20−80 °C at a frequency of 1 Hz and a heating rate of 3 °C/min. For the DMA study, the samples were molded into films on a hot press under a pressure of 10 MPa at 190 °C for 3 min and further quenched into ice water. The obtained films were amorphous on the basis of the WAXD experiment.

Thermogravimetry Analysis (TGA). TGA measurement was performed on a TA Q50 instrument. All operations were performed under nitrogen purge. The sample was heated from room temperature to 580 at 20 °C/min.

RESULTS AND DISCUSSION

Dispersion of ome-POSS in the PLLA Matrix. It is clear that the dispersion of POSS in the polymer matrix must influence the physical properties of biodegradable polymer significantly; therefore, the dispersion of ome-POSS in the PLLA matrix was studied with SEM and TEM first in this work. Figure 1a shows the SEM image of a POSS-5 sample as an example. It can be seen from Figure 1a that several white particles are randomly dispersed within the PLLA matrix, corresponding to the aggregation of ome-POSS with the size around 200 nm. Figure 1b demonstrates a typical TEM image of the ultrathin section for a POSS-5 sample, from which the ome-POSS regular crystals are observed with the size of ca. 200 nm. Similar results are also found for the POSS-2 and POSS-8 samples. For brevity, the results are not shown here. Both the SEM and TEM observations suggest a homogeneous dispersion of ome-POSS in the PLLA matrix. The formation of submicrometer aggregates of ome-POSS indicates that there is somewhat compatibility between ome-POSS and the PLLA matrix; however, such compatibility is limited since the interaction between the methyl group of ome-POSS and the PLLA matrix may not be strong. It should be noted that the dispersion of ome-POSS is better in PLLA than in some other polymer matrixes such as linear low-density PE (LLDPE) and

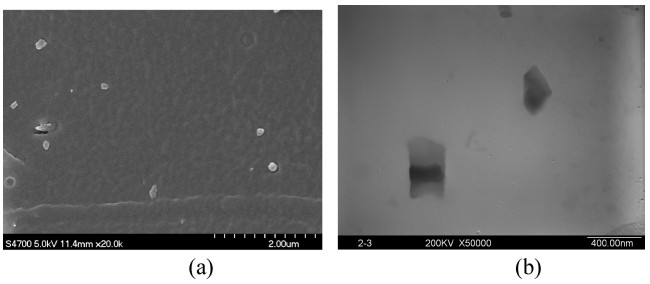

Figure 1. (a) SEM image and (b) TEM image of POSS-5.

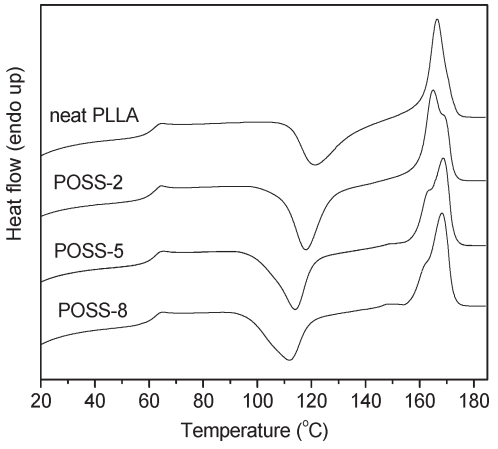

Figure 2. DSC heating traces of neat PLLA and its nanocomposites at 20 °C/min from the amorphous state.

PP. In the LLDPE/ome-POSS composites[49] and PP/ome-POSS composites[41] prepared via melt compounding, the aggregation of ome-POSS was more serious, and the size of the aggregates was even more than 10 μm. In previous work, a fine dispersion of oib-POSS was achieved in the PLLA matrix since the submicrometer aggregates with dimensions ranging from around 100 to 200 nm were found.[48] It is clear that the dispersion of oib-POSS is slightly better in the PLLA/oib-POSS nanocomposites prepared via solution and coagulation method than that of ome-POSS in the PLLA/ome-POSS nanocomposites prepared via simple melt compounding. In brief, the aggregation of POSS in the polymer matrix depends on not only the type of POSS but also the polymer matrix as well as the method of preparing polymer/POSS nanocomposites.

Nonisothermal Cold Crystallization of Neat PLLA and Its Nanocomposites. It is interesting to study the effect of ome-POSS on the nonisothermal crystallization behavior of PLLA in the PLLA/ome-POSS nanocomposites. Nonisothermal cold crystallization behavior of neat PLLA and the PLLA/ome-POSS nanocomposites was studied with DSC first in this work. Figure 2 shows the DSC heating traces of neat PLLA and its nanocomposites from the amorphous state at 20 °C/min. It is obvious that the incorporation of ome-POSS shows little effect on the glass transition temperature (T_g) of PLLA, which is around 62.5 °C despite the ome-POSS loading. Neat PLLA exhibits a cold crystallization onset temperature (T_{on}) of 106.0 °C and a cold crystallization peak temperature (T_{ch}) of 121.6 °C with crystallization enthalpy (ΔH_{ch}) being 36.7 J/g; however, both T_{on} and T_{ch} shift gradually to lower temperature range with increasing the ome-POSS content in the PLLA/ome-POSS nanocomposites. In the case of POSS-8, T_{on} shifts to around 89.5 °C; moreover, T_{ch} shifts to around 111.9 °C, which is nearly 10 °C lower than that of neat PLLA. Neat PLLA has a melting point (T_m) of 166.4 °C with heat of fusion (ΔH_m) being 37.2 J/g. For the PLLA/ome-POSS nanocomposites, T_m varies between 165.0 to 168.7 °C slightly, and ΔH_m varies slightly between 40.6 and 42.5 J/g. It should also be noted from Figure 2 that double melting peaks or one major melting peak with a shoulder are found for the PLLA/ome-POSS nanocomposites while only one melting peak is observed for neat PLLA. Such results may be explained as follows. The cold crystallization of PLLA occurred at lower temperature range in the nanocomposites due to the nucleation effect of ome-POSS relative to neat PLLA, thereby resulting in that the crystals were not so perfect in the nanocomposites as in neat PLLA. The unstable crystals may undergo melting, recrystallization, and remelting upon further heating in DSC; therefore, double melting peaks or one major melting peak with a shoulder are observed in the PLLA/ome-POSS nanocomposites. On the basis of the heat of fusion of 100% crystalline (ΔH_m^o) PLLA (93 J/g),[50] the degree of crystallinity (W_c) of neat PLLA and its nanocomposites are determined and normalized with respect to the composition of each component in the composites. It is found that W_c is around 40% for neat PLLA, increasing to be around 46% for the PLLA/ome-POSS nanocomposites despite the ome-POSS loading. It is clear that the presence of ome-POSS enhances nonisothermal cold crystallization of PLLA significantly in the nanocomposites relative to neat PLLA. All of the above-mentioned parameters are summarized in Table 1 for comparison.

Nonisothermal Melt Crystallization of Neat PLLA and Its Nanocomposites. Nonisothermal melt crystallization of neat PLLA and its nanocomposites was further studied with DSC. Two different cooling rates, i.e., 5 and 15 °C/min were used in this work to study the effect of ome-POSS on the nonisothermal melt crystallization of PLLA in the PLLA/ome-POSS nanocomposites. Figure 3a shows the DSC cooling traces of neat PLLA and its nanocomposites at 5 °C/min. As shown in Figure 3a, neat PLLA shows a melt crystallization peak temperature (T_{cc}) at around 96.0 °C with crystallization enthalpy (ΔH_{cc}) being around 7.2 J/g; however, T_{cc} values shift gradually to 103.1, 106.2, and 106.9 °C with the values of ΔH_{cc} being around 38.3, 39.6, and 40.9 J/g for POSS-2, POSS-5, and POSS-8, respectively. The values of W_c are determined to be around 8.3%, 42.4%, 45.0%, and 47.8% for neat PLLA, POSS-2, POSS-5, and POSS-8, respectively. It is clear that T_{cc} is increased apparently in the PLLA/ome-POSS nanocomposites than in neat PLLA; moreover, ΔH_{cc} and W_c are increased significantly in the PLLA/ome-POSS nanocomposites than in neat PLLA. However, the variation of the ome-POSS loading shows no significant influence on the nonisothermal melt crystallization behavior of PLLA in the nanocomposites, especially when the ome-POSS loading is increased from 5 to 8 wt %. The aforementioned results indicate that nonisothermal melt crystallization of PLLA is enhanced by the presence of ome-POSS in the nanocomposites and influenced slightly by the ome-POSS loading. In addition, nonisothermal melt crystallization of neat PLLA and its nanocomposites was further studied at a relatively high cooling rate of 15 °C/min. As shown in Figure 3b, the nonisothermal melt crystallization of PLLA is hardly observed for neat PLLA at 15 °C/min, while it can still be easily observed in the PLLA/ome-POSS nanocomposites despite the ome-POSS loading. It is clear from Figure 3b that the nonisothermal melt crystallization of PLLA in the nanocomposites is mainly induced by the presence

Table 1. Summary of Some Characteristic Parameters for Neat PLLA and Its Nanocomposites during Nonisothermal Cold Crystallization at 20 °C/min

samples	T_g (°C)	T_{on} (°C)	T_{ch} (°C)	ΔH_{ch} (J/g)	T_m (°C)	ΔH_m (J/g)	W_c (%)
neat PLLA	62.1	106.0	121.6	36.7	166.4	37.2	40.0
POSS-2	62.8	95.4	118.0	42.4	165.0	42.5	46.6
POSS-5	62.5	91.2	114.0	40.5	168.7	40.9	46.3
POSS-8	62.6	89.5	111.9	38.7	168.3	40.6	47.4

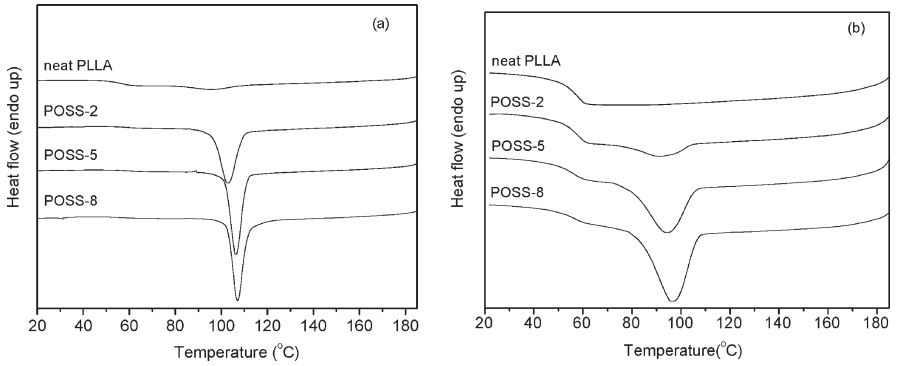

Figure 3. Nonisothermal melt crystallization of neat PLLA and its nanocomposites at different cooling rates: (a) 5 and (b) 15 °C/min.

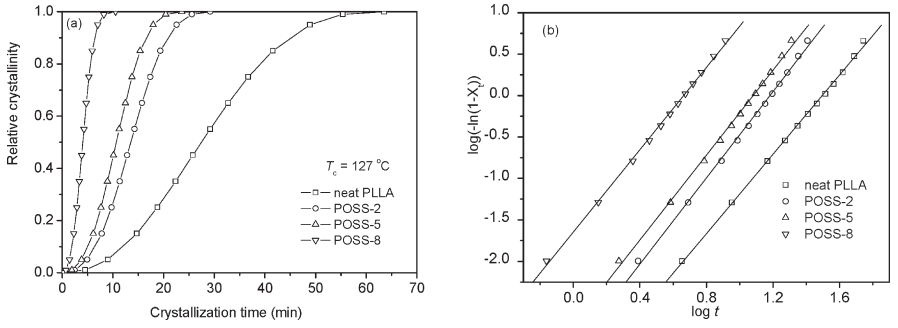

Figure 4. (a) Variation in relative crystallinity with crystallization time for neat PLLA and its nanocomposites at 127 °C and (b) the related Avrami plots.

of ome-POSS relative to neat PLLA at a high cooling rate of 15 °C/min, suggesting that nonisothermal melt crystallization of PLLA may be enhanced significantly in the nanocomposites at high cooling rate. It can thus be concluded that both nonisothermal cold and melt crystallization of PLLA are enhanced significantly in the PLLA/ome-POSS nanocomposites relative to neat PLLA, indicating that ome-POSS may act as an effective nucleating agent during the nonisothermal cold and melt crystallization of PLLA.

Isothermal Melt Crystallization Kinetics of Neat PLLA and Its Nanocomposites. Nonisothermal cold and melt crystallization behaviors of neat PLLA and the PLLA/ome-POSS nanocomposites were studied with DSC in the above sections. In this section, the effect of ome-POSS on the isothermal melt crystallization kinetics of PLLA in the PLLA/ome-POSS nanocomposites was further investigated with DSC. As introduced in the Experimental Section, the overall isothermal crystallization kinetics of neat PLLA and its nanocomposites were studied with DSC in a temperature range from 119 to 127 °C. The effect of the ome-POSS loading on the isothermal melt crystallization of PLLA was studied first. Figure 4a shows the plots of relative crystallinity against crystallization time at 127 °C as an example. It is clear from Figure 4a that all these curves have the similar sigmoid shape; moreover, the corresponding crystallization time for the PLLA/ome-POSS nanocomposites becomes shorter with increasing the ome-POSS loading. For instance, it took neat PLLA about 64 min to finish crystallization at 127 °C, but for the POSS-2, POSS-5, and POSS-8 samples, the time required to finish crystallization became only around 29, 23, and 11 min, respectively. It is obvious that the incorporation of ome-POSS enhances the isothermal melt crystallization of PLLA remarkably when compared with neat PLLA; moreover, with increasing the ome-POSS content, the isothermal crystallization of PLLA becomes faster.

The well-known Avrami equation is often used to analyze the isothermal crystallization kinetics of polymers;[51,52] it assumes that the relative degree of crystallinity develops with crystallization time as

$$1 - X_t = \exp(-kt^n) \quad (1)$$

where X_t is the relative degree of crystallinity at crystallization time (t), n is the Avrami exponent depending on the nature of nucleation and growth geometry of the crystals, and k is the crystallization rate constant involving both nucleation and growth rate parameters.[53,54] In the case of the DSC experiment, X_t at t is defined as the ratio of the area under the exothermic

curve between the onset crystallization time and t to the whole area under the exothermic curve from the onset crystallization time to the end crystallization time. Figure 4b shows the Avrami plots of neat PLLA and its nanocomposites crystallized at 127 °C as an example, from which the Avrami parameters n and k can be obtained from the slopes and the interceptions, respectively.

The Avrami parameters are summarized in Table 2 for neat PLLA and its nanocomposites crystallized at different crystallization temperatures (T_c). It can be seen that the average values of n are around 2.5 and almost unchanged with the addition of ome-POSS, suggesting that the incorporation of ome-POSS may not change the crystallization mechanism of PLLA in the PLLA/ome-POSS nanocomposites.[53] The k values are also listed in Table 2. However, it should be noted that it is difficult to compare the overall crystallization rate directly from the k values because the unit of k is min^{-n} and n is not constant. Thus, the crystallization half-time ($t_{0.5}$), the time required to achieve 50% of the final crystallinity of the samples, is introduced for the discussion of crystallization kinetics. The crystallization rate can thus be easily described by the reciprocal of $t_{0.5}$. The value of $t_{0.5}$ is calculated by the following equation:

$$t_{0.5} = \left(\frac{\ln 2}{k}\right)^{1/n} \quad (2)$$

Parts a and b of Figure 5 illustrate the variations of $t_{0.5}$ and $1/t_{0.5}$ with T_c for neat PLLA and its nanocomposites, respectively, from which the effects of T_c and the ome-POSS loading on the variation of overall crystallization rate can be obtained clearly. As shown in Figure 5, the $t_{0.5}$ values increase while the $1/t_{0.5}$ values decrease with increasing T_c for both neat PLLA and its nanocomposites, indicating that the overall isothermal crystallization rate decreases with increasing T_c. Such results are reasonable since it is difficult for the samples to nucleate at high T_c, thereby resulting in the reduction of the overall crystallization rate. In addition, the $t_{0.5}$ values are smaller in the nanocomposites than in neat PLLA at a given T_c, indicating again that the isothermal melt crystallization of PLLA is accelerated by the presence of ome-POSS. Such results suggest that ome-POSS nanocomposites.

Table 2. Summary of Isothermal Melt Crystallization Kinetics Parameters of Neat PLLA and Its Nanocomposites at Different T_cs Based on the Avrami Equation

samples	T_c (°C)	n	k (min^{-n})
neat PLLA	119	2.5	$4.95 \times 10-3$
	121	2.5	3.07×10^{-3}
	123	2.5	1.74×10^{-3}
	125	2.4	5.46×10^{-4}
	127	2.4	2.62×10^{-4}
POSS-2	119	2.5	1.29×10^{-2}
	121	2.6	4.43×10^{-3}
	123	2.5	4.05×10^{-3}
	125	2.5	2.58×10^{-3}
	127	2.6	8.41×10^{-4}
POSS-5	119	2.6	1.97×10^{-2}
	121	2.6	6.65×10^{-3}
	123	2.6	4.51×10^{-3}
	125	2.6	2.24×10^{-3}
	127	2.6	1.71×10^{-3}
POSS-8	119	2.5	1.29×10^{-1}
	121	2.4	8.00×10^{-2}
	123	2.4	5.15×10^{-2}
	125	2.4	3.14×10^{-2}
	127	2.5	2.25×10^{-2}

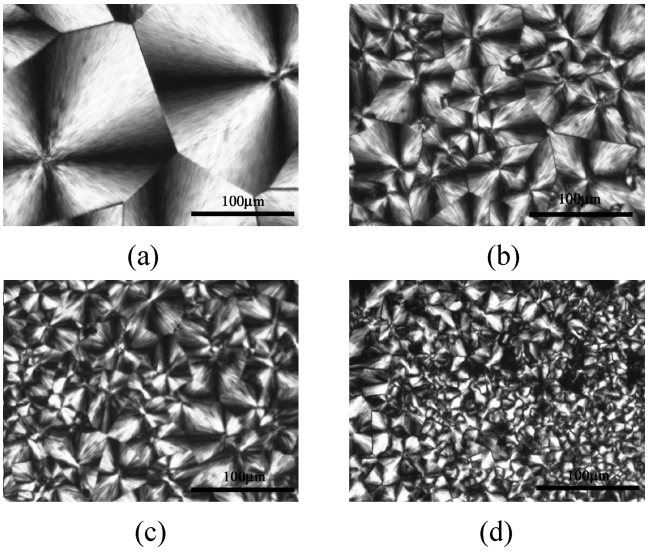

Figure 6. POM images of neat PLLA and its nanocomposites crystallized at 125 °C; (a) neat PLLA for 90 min, (b) POSS-2 for 35 min, (c) POSS-5 for 18 min, and (d) POSS-8 for 12 min.

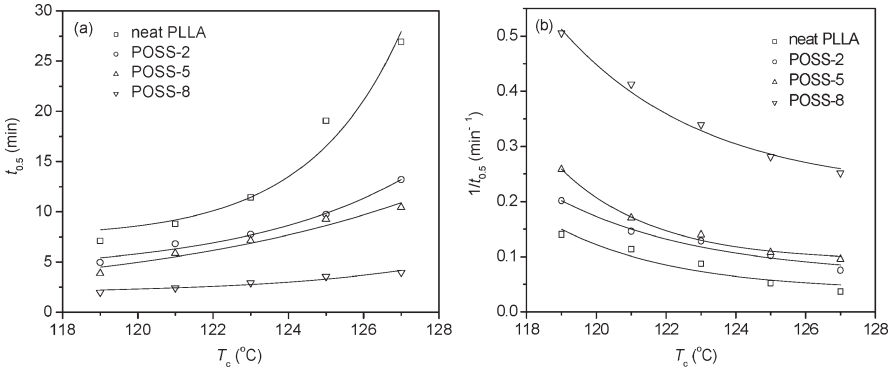

Figure 5. Variations of (a) $t_{0.5}$ and (b) $1/t_{0.5}$ with T_c for neat PLLA and its nanocomposites.

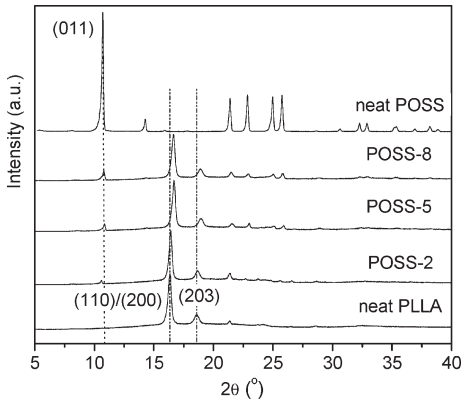

Figure 7. WAXD patterns of neat PLLA and its nanocomposites.

may act as an effective nucleating agent during the isothermal melt crystallization of PLLA in the PLLA/ome-POSS nanocomposites. As shown in Figure 5b, the $1/t_{0.5}$ values increase with increasing the ome-POSS loading in the PLLA/ome-POSS nanocomposites at a given T_c, suggesting that the ome-POSS loading has a significant effect on the crystallization of PLLA. In brief, the overall isothermal melt crystallization of PLLA is accelerated by the presence of ome-POSS in the PLLA/ome-POSS nanocomposites relative to neat PLLA; moreover, the enhancement of the overall crystallization rate of PLLA is influenced by the ome-POSS loading. The DSC results reported herein are consistent with the spherulitic morphology study in the following section.

Figure 6 displays the spherulitic morphology of neat PLLA and its nanocomposites crystallized at 125 °C. As shown in Figure 6a, the well-developed spherulites of neat PLLA grow to a size of about 150 μm in diameter, and the boundaries are clear. Parts b, c, and d in Figure 6 illustrate the POM images of the nanocomposites with the ome-POSS loading from 2 to 8 wt % respectively. It is obvious that the number of PLLA spherulites is greater in the PLLA/ome-POSS nanocomposites than in neat PLLA; moreover, the size of PLLA spherulites is smaller in the PLLA/ome-POSS nanocomposites than in neat PLLA. In addition, the PLLA spherulites boundaries become obscure in the PLLA/ome-POSS nanocomposites, especially at high ome-POSS loading. Such variations indicate that the nucleation density of PLLA spherulites increases dramatically in the PLLA/ome-POSS nanocomposites because of the nucleating agent effect of ome-POSS. In sum, the presence of ome-POSS and their contents in the PLLA matrix are the main factors, which influence the spherulitic morphology and the overall crystallization process of PLLA significantly.

It is interesting to study the effect of ome-POSS on the crystal structure of PLLA in the PLLA/ome-POSS nanocomposites. As introduced in the Experimental Section, WAXD experiments were performed to investigate the crystal structures of neat PLLA and its nanocomposites at different ome-POSS loading. It should be noted that all the samples crystallized at 128 °C; therefore, both neat PLLA and its nanocomposites crystallize in α form. In Figure 7, the presence of a number of strong diffraction peaks shows that ome-POSS are highly crystalline. Moreover, the characteristic diffraction peak of ome-POSS at around 11.0°, as reported by Barry[55] and Hsiao,[56] also appears in the PLLA/ome-POSS nanocomposites, suggesting that ome-POSS may exist as the separate crystals or ome-POSS particles are able to crystallize when they are dispersed in the PLLA matrix. Similar results are also found in the PLLA/oib-POSS nanocomposites.[48] For neat PLLA, two sharp characteristic diffraction peaks are shown at 16.25 and 18.57°, corresponding to (200)/(110) and (203) planes, respectively.[57] In addition, for the PLLA/ome-POSS nanocomposites, the similar diffraction patterns are observed in Figure 7, indicating that incorporating with ome-POSS does not modify the crystal structure of PLLA; however, the two sharp characteristic diffraction peaks of PLLA shift slightly to higher 2θ range, which must influence the crystal lattice parameters of PLLA. In brief, the crystal structure of PLLA remains unchanged despite the addition of ome-POSS in the PLLA/ome-POSS nanocomposites.

Effect of ome-POSS on the Dynamic Mechanical Properties and Thermal Stability of PLLA. In this section, the effect of ome-POSS on the dynamic mechanical properties and thermal stability of PLLA was investigated. Parts a and b of Figure 8 show the temperature dependence of storage modulus (E') and tan δ, the ratio of loss modulus to storage modulus, of neat PLLA and the PLLA/ome-POSS nanocomposites, respectively. It is obvious from Figure 8a that the storage modulus increases significantly after the incorporation of ome-POSS at low temperature in the glass state (0−60 °C), indicating that the addition of ome-POSS particles induces a reinforcement effect. The value of E' is around 1879 MPa for neat PLLA at 20 °C, which increases to around 2084, 2144, and 2187 MPa, respectively, with increasing the ome-POSS loading from 2 to 8 wt %. It should also be mentioned that the increase in E' is apparent with the ome-POSS loadings from 0 to 2 wt %; however, the difference is slight with further increasing ome-POSS loading from 2 to 8 wt % in the PLLA matrix, indicating that such effect is more pronounced at lower ome-POSS content. The significant improvement in E' may be ascribed to the combined effect of high performance and fine dispersion of ome-POSS in the PLLA matrix. Similar improvement in E' was also found in the LLDPE/ome-POSS nanocomposites.[49] Furthermore, it is seen that both neat PLLA and the PLLA/ome-POSS nanocomposites exhibit a sharp reduction of elastic modulus around 70 °C, corresponding to the glass transition of PLLA. In addition, the storage modulus difference between neat PLLA and the PLLA/ome-POSS nanocomposites is very small and tends to zero in the temperature range of 70 to 80 °C, suggesting that the nanocomposites stiffness become matrix dependent at the rubbery state. From Figure 8b, the glass transition temperatures for neat PLLA and the PLLA/ome-POSS nanocomposites are estimated to be around 70 °C, indicating that the presence of ome-POSS does not significantly influence the segmental motion of PLLA in the nanocomposites.

The effect of ome-POSS on the thermal stability of PLLA was further investigated. Figure 9 shows the TGA curves of neat PLLA and its nanocomposites. As introduced in the Experimental Section, all the samples were heated from room temperature to 580 °C in nitrogen atmosphere at 20 °C/min. It can be seen from Figure 9 that both neat PLLA and its nanocomposites present a similar degradation profile, suggesting that the presence of ome-POSS does not alter the degradation mechanism of the PLLA matrix. As shown in Figure 9, the degradation temperature at 5% weight loss (T_d) is about 347 °C for neat PLLA, while T_d is about 222 °C for pure ome-POSS. For the PLLA/ome-POSS nanocomposites, T_ds are 294, 305, and 321 °C with increasing the ome-POSS loading from 2 to 8 wt %, respectively, indicating that the incorporation of ome-POSS reduces slightly the thermal stability of the PLLA matrix, especially at high ome-POSS loading. Similar reduced thermal stability was also found in the

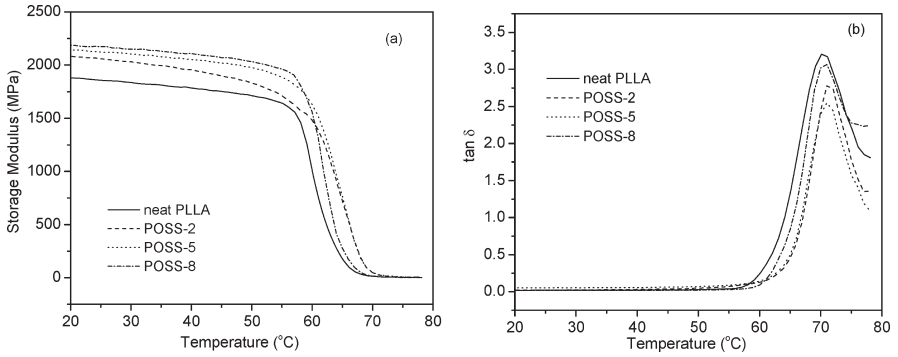

Figure 8. Temperature dependence of (a) storage modulus and (b) tan δ for neat PLLA and its nanocomposites.

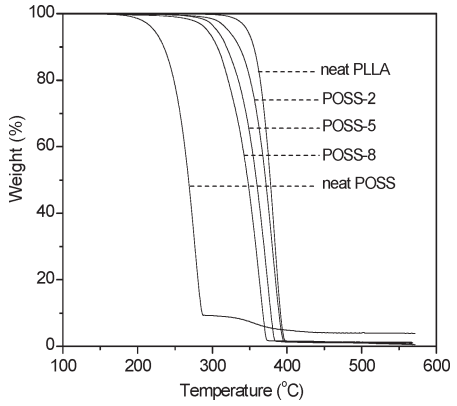

Figure 9. TGA curves of neat ome-POSS, neat PLLA, and their nanocomposites.

iPP/ome-POSS nanocomposites.[58] T_d was about 395 °C for pure iPP, whereas in the iPP/ome-POSS nanocomposites, T_d was in the range of 320−348 °C depending on the ome-POSS loading.[58] The slight reduced thermal stability indicates that there are no chemical bonds or strong interaction between ome-POSS and the PLLA matrix.

CONCLUSIONS

Biodegradable PLLA/ome-POSS nanocomposites were prepared successfully in this work via simple melt compounding at various ome-POSS loadings. SEM and TEM observations indicate that ome-POSS are homogeneously dispersed in the PLLA matrix. Effect of ome-POSS on the nonisothermal cold and melt crystallization behaviors, isothermal melt crystallization kinetics, spherulitic morphology, crystal structure, dynamic mechanical properties, and thermal stability of PLLA in the PLLA/ome-POSS nanocomposites was investigated in detail with DSC, POM, WAXD, DMA, and TGA and compared with those of neat PLLA. It is found that the presence of ome-POSS enhances nonisothermal cold and melt crystallization behaviors of PLLA in the nanocomposites apparently relative to neat PLLA. In particular, nonisothermal melt crystallization of PLLA may be induced by the presence of ome-POSS in the PLLA/ome-POSS nanocomposites at a relatively high cooling rate of 15 °C/min, while neat PLLA can hardly crystallize at the same cooling rate. Isothermal melt crystallization kinetics of neat PLLA and its nanocomposites was studied with DSC at various crystallization temperatures and analyzed by the Avrami equation. The overall crystallization rates are faster in the PLLA/ome-POSS nanocomposites than in neat PLLA and increase with increasing the ome-POSS loading; however, the crystallization mechanism of PLLA remains unchanged despite the presence of ome-POSS. The POM results show that the number of PLLA spherulites is greater in the PLLA/ome-POSS nanocomposites than in neat PLLA; moreover, the size of PLLA spherulites is smaller in the PLLA/ome-POSS nanocomposites than in neat PLLA. The increased nucleation density of PLLA spherulites in the nanocomposites indicates that ome-POSS may act as an effective nucleating agent during the crystallization process of PLLA. On the basis of the WAXD study, it can be concluded that the incorporation of ome-POSS does not modify the crystal structure of PLLA in the nanocomposites relative to neat PLLA. The storage modulus has been apparently improved in the PLLA/POSS nanocomposites with respect to neat PLLA, while the glass transition temperatures vary slightly between neat PLLA and the PLLA/POSS nanocomposites. The similar degradation profiles of neat PLLA and its nanocomposites suggest that ome-POSS does not alter the degradation mechanism of the PLLA matrix; however, the thermal stability of PLLA matrix is reduced slightly in the PLLA/POSS nanocomposites.

AUTHOR INFORMATION

Corresponding Author

*Fax: +86-10-64413161. E-mail: qiuzb@mail.buct.edu.cn.

ACKNOWLEDGMENT

The authors thank Biomer, Germany for kindly supplying PLLA sample. Part of this work is financially supported by the National Natural Science Foundation, China (20974012), the Fundamental Research Funds for the Central Universities (ZZ1005), and Program for Changjiang Scholars and Innovative Research Team in University (IRT0706).

REFERENCES

(1) Garlotta, D. *J. Polym. Environ.* **2001**, *9*, 63–84.
(2) Bogaert, J.; Coszac, P. *Macromol. Symp.* **2000**, *153*, 287–303.
(3) Drumright, R.; Gruber, P.; Henton, D. *Adv. Mater.* **2000**, *12*, 1841–1846.
(4) Ikada, Y.; Tsuji, H. *Macromol. Rapid Commun.* **2000**, *21*, 117–132.
(5) De Santis, P.; Kovacs, A. *Biopolymers* **1968**, *6*, 299–306.
(6) Kawai, T.; Rahman, N.; Matsuba, G.; Nishida, K.; Kanaya, T.; Nakano, M.; Okamoto, H.; Kawada, J.; Usuki, A.; Honma, N.; Nakajima, K.; Matsuda, M. *Macromolecules* **2007**, *40*, 9463–9469.
(7) Qiu, X.; Redwine, D.; Gobbi Anuttra Nuamthanom, G.; Rinaldi, P. *Macromolecules* **2007**, *40*, 6879–6884.

(8) Pan, P.; Zhu, B.; Kai, W.; Dong, T.; Inoue, Y. *Macromolecules* **2008**, *41*, 4296–4304.
(9) Pan, P.; Liang, Z.; Zhu, Bo.; Dong, T.; Inoue, Y. *Macromolecules* **2009**, *42*, 3374–3380.
(10) Zhang, J.; Duan, Y.; Sato, H.; Tsuji, H.; Noda, I.; Yan, S.; Ozaki, Y. *Macromolecules* **2005**, *38*, 8012–8021.
(11) Yasuniwa, M.; Tsubakihara, S.; Sugimoto, Y.; Nakafuku, C. *J. Polym. Sci., Part B: Polym. Phys.* **2004**, *42*, 25–32.
(12) Pan, P.; Kai, W.; Zhu, B.; Dong, T.; Inoue, Y. *Macromolecules* **2007**, *40*, 6898–6905.
(13) Yasuniwa, M.; Sakamo, K.; Ono, Y.; Kawahara, W. *Polymer* **2008**, *49*, 1943–1951.
(14) Di Lorenzo, M. *Eur. Polym. J.* **2005**, *41*, 569–575.
(15) Iannace, S; Nicolais, L. *Polymer* **1997**, *38*, 4003–4009.
(16) Lu, J.; Qiu, Z.; Yang, W. *Polymer* **2007**, *48*, 4196–4204.
(17) Wu, C.; Liao, H. *Polymer* **2007**, *48*, 4449–4458.
(18) Chang, J.; An, Y.; Sur, G. *J. Polym. Sci., Part B: Polym. Phys.* **2003**, *41*, 94–103.
(19) Fukuda, N.; Tsuji, H. *J. Appl. Polym. Sci.* **2005**, *96*, 190–199.
(20) Thostenson, T.; Ren, Z.; Chou, T. *Compos. Sci. Technol.* **2001**, *61*, 1899–1912.
(21) http://www.nanoclay.com.
(22) Zhao, Y.; Qiu, Z.; Yang, W. *J. Phys. Chem. B* **2008**, *112*, 16461–16468.
(23) Zhang, D.; Kandadai, M.; Cech, J.; Roth, S.; Curran, S. *J. Phys. Chem. B* **2006**, *110*, 12910–12915.
(24) Shieh, T.; Liu, L. *J. Polym. Sci., Part B: Polym. Phys.* **2007**, *45*, 1870–1881.
(25) Kim, S.; Park, B.; Yoon, J.; Jin, H. *Eur. Polym. J.* **2007**, *43*, 1729–1735.
(26) Ogata, N.; Jimenez, G.; Kawai, H.; Ogihara, T. *J. Polym. Sci., Part B: Polym. Phys.* **1997**, *35*, 389–396.
(27) Sinha Ray, S.; Yamada, K.; Okamoto, M.; Ueda, K. *Nano Lett.* **2002**, *2*, 1093–1906.
(28) Pluta, M.; Paul, M.; Alexandre, M.; Dubois, P.; Galeski, A. *J. Appl. Polym. Sci.* **2002**, *86*, 1497–1506.
(29) Maiti, P.; Yamada, K.; Okamoto, M.; Ueda, K.; Okamato, K. *Chem. Mater.* **2002**, *14*, 4654–4661.
(30) Baney, R. H.; Itoh, M.; Sakakibara, A.; Suzuki, T. *Chem. Rev.* **1995**, *95*, 1409–1430.
(31) Harrison, P. *J. Organomet. Chem.* **1997**, *542*, 141–183.
(32) Li, G.; Wang, L.; Ni, H.; Pittman *J. Inorg. Organomet. Polym.* **2001**, *11*, 123–154.
(33) Liu, Y.; Yang, X.; Zhang, W.; Zheng, S. *Polymer* **2006**, *47*, 6814–6825.
(34) Ni, Y.; Zheng, S. *J. Polym. Sci., Part B: Polym. Phys.* **2007**, *45*, 2201–2214.
(35) Goffin, A.; Duquesne, E.; Moins, S.; Alexandre, M.; Dubois, P. *Eur. Polym. J.* **2007**, *43*, 4103–4113.
(36) Lin, H.; Wu, S.; Huang, P.; Huang, C.; Kuo, S.; Chang, F. *Macromol. Rapid Commun.* **2008**, *27*, 1550–1555.
(37) Kim, B.; Mather, P. *Macromolecules* **2006**, *39*, 9253–9260.
(38) Choi, J.; Kim, S.; Laine, R. *Macromolecules* **2004**, *37*, 99–109.
(39) Lee, Y.; Kuo, S.; Huang, W.; Lee, H.; Chang, F. *J. Polym. Sci., Part B: Polym. Phys.* **2004**, *42*, 1127–1136.
(40) Zheng, L.; Farris, R.; Coughlin, E. *Macromolecules* **2001**, *34*, 8034–8039.
(41) Fina, A.; Tabuani, D.; Frache, A.; Camino, G. *Polymer* **2005**, *46*, 7855–7866.
(42) Lee, Y.; Huang, J.; Kuo, S.; Chang, F. *Polymer* **2005**, *46*, 10056–10065.
(43) Zhao, Y.; Schiraldi, D. *Polymer* **2005**, *46*, 11640–11647.
(44) Sharon, Y.; Cohen, R.; Boyce, M. *Polymer* **2007**, *48*, 1410–1418.
(45) Zhang, Y.; Lee, S.; Yoonessi, M.; Liang, K.; Pittman, C. *Polymer* **2006**, *47*, 2984–2996.
(46) Kopesky, E.; McKinley, G.; Cohen, R. *Polymer* **2006**, *47*, 299–309.
(47) Qiu, Z.; Pan, H. *Compos. Sci. Technol.* **2010**, *70*, 1089–1094.
(48) Pan, H.; Qiu, Z. *Macromolecules* **2010**, *43*, 1499–1506.
(49) Hato, M.; Sinha Ray, S.; Luyt, A. *Macromol. Mater. Eng.* **2008**, *293*, 752–762.
(50) Fischer, E.; Sterzel, H.; Wegner, G. *Kolloid Z. Z. Polym.* **1973**, *251*, 980–990.
(51) Avrami, M. *J. Chem. Phys.* **1940**, *8*, 212–224.
(52) Avrami, M. *J. Chem. Phys.* **1941**, *9*, 177–184.
(53) Kamal, M.; Chu, E. *Polym. Eng. Sci.* **1983**, *23*, 27–31.
(54) Wunderlich, B. In *Macromolecular Physics*; Academic Press: New York, 1976; Vol. 2, p 147.
(55) Barry, A. J.; Daudt, W. H.; Domincone, J. J.; Gilkey, J. W. *J. Am. Chem. Soc.* **1955**, *77*, 4248–4252.
(56) Fu, B.; Yang, L.; Somani, R.; Zong, S.; Hsiao, B.; Phillips, S.; Blamski, R.; Ruth, P. *J. Polym. Sci., Part B: Polym. Phys.* **2001**, *39*, 2727–2739.
(57) Hoogsteen, W.; Postema, A.; Pennings, A.; Ten Brinke, G.; Zugenmaier, P. *Macromolecules* **1990**, *23*, 634–642.
(58) Chen, J.; Chiou, Y. *J. Polym. Sci., Part B: Polym. Phys.* **2006**, *44*, 2122–2134.